Asymptotic Fourier decomposition of tooth forces in terms of convolved air gap field harmonics for noise diagnosis of electrical machines

M. van der Giet, R. Rothe, K. Hameyer
Institute of Electrical Machines, RWTH Aachen University, Schinkelstraße, D-52056 Aachen, Germany
E-mail: Michael.vanderGiet@iem.rwth-aachen.de

***Abstract*: The electromagnetic excited audible noise of electrical machines can be mostly attributed to to radial forces on stator tooth-heads. Classical noise analysis approaches focus then on the wave numbers and frequencies of the spectral decomposition of the air gap field $b(x,t)$. Numerical approaches on the other hand, make it possible to compute the magnetic field, and thus the force amplitudes, with a much greater accuracy. The approach presented in this paper combines the benefits of both approaches by firstly performing a numerical field analysis, then transforming the radial air gap field into the frequency domain, and finally performing a matrix convolution. The latter operation reveals the relationship between air gap field harmonics and the corresponding force waves acting on the stator teeth. The proposed method is demonstrated on a PMSM motor, and numerical results are given.**

***Keywords*: noise and vibration, electrical machines, analytical methods, FEM**

I. Introduction

The reduction of audible noise in electrical machines is attracting more and more attention. Designing low noise electrical machines requires a good understanding of the causes of noise excitation.

Classical analytical approaches for noise analysis in electrical machines rely on the identification of the space and time harmonics in the air gap field that generate radial magnetic force waves [1], [2]. The causality relation between force waves and field harmonics can be traced back this way. The drawback of such methods, however, is the limited accuracy of the air gap field and magnetic force wave amplitudes.

Numerical simulations, with e.g. the Finite Element (FE) method, are able to capture finer details and allow an accurate determination of air gap field and magnetic force amplitudes [2], [3] and [4]. Under the standard linear assumption, the vibroacoustic problem is most commonly solved in the frequency domain, either by modal analysis and superposition, or by immediate harmonic analysis. In both cases, the computed electromagnetic force excitations are transformed into the frequency domain. Besides the Fourier transform of time waves, spatial waves are also transformed in order to identify the spatial wave numbers of the air gap field. Comparing the wave numbers and frequencies with those obtained from analytical models, it is possible to identify which magnetic field harmonic predominantly contribute to a given force wave [5].

However, it is not possible by this approach to find out the exact composition of each force wave. The approach presented in this paper overcomes this fundamental drawback by Fourier transforming the magnetic field in time and space directly so as to obtain a representation of the air gap field as a function of wave numbers and frequencies.

The outline of this paper reads as follows: First the analysis of magnetic force waves by means of the analytical model is explained. Afterwards a brief review of the two-dimensional discrete Fourier transform (2D DFT) and the usage of space vectors is given. The subsequent section presents numerical results for one particular example machine, and a summary concludes the paper.

II. Generation of magnetic force waves

The air gap field in electrical machines cause force densities on the permeable material of the stator and rotor teeth. Featuring different frequency components, these forces are responsible for mechanical vibrations that radiate air-borne sound.

Magnetic forces acting on a given medium are the divergence of the electromechanical tensor of that medium. Each medium has its own electromechanical tensor, and that of empty space, or air, is the celebrated Maxwell stress tensor [6]. In consequence, magnetic forces come under volume and surface density form. In saturable non-conducting materials, the volume density is basically related with the gradient of the magnetic reluctivity, and it is usually negligible with respect to the surface force density. The latter, located at material discontinuities (e.g. on the stator surface in the air gap), is the divergence in the sense of distribution of the electromechanical tensor. It can be shown [7] that it has a normal component only, whose amplitude is

$$P_r = \left[B_r(H_{1r} - H_{2r}) - (w_1' - w_2')\right], \tag{1}$$

where B_r is the radial magnetic flux density at the interface between the stator and the air gap. H_{1r} and H_{2r} are the radial magnetic field strength in the air and in the stator iron, respectively. The magnetic co-energy density w' is related to the magnetic energy density w by

$$w' = H(B)\cdot B - w(B) = H(B)\cdot B - \int_0^{|B|} |H(x)|dx \tag{2}$$

Due to the constant magnetic permeability of air, w_1' is

$$w_1' = H\cdot B - \frac{1}{2}H\cdot B = \frac{|B|^2}{2\mu_0}, \tag{3}$$

where μ_0 denotes the magnetic permeability of vacuum. If the permeability of the iron cannot be considered constant, the magnetic energy term of the iron has to be determined by means of numerical integration along the BH-curve, otherwise, i.e. in the linear case, (1) can be simplified to

$$P_r = \frac{1}{2}\left[B_r(H_{1r} - H_{2r}) - H_t(B_{1t} - B_{2t})\right] \tag{4}$$

If in addition, the permeability of the iron is sufficiently large and the magnetic field strength in the iron can be neglected, the magnetic force density is finally approximated by

$$P_r = \frac{B_r^2}{2\mu_0}. \tag{5}$$

In steady state operation, the air gap field is periodic in time and space, and it is commonly described by a Fourier series of a one-dimensional wave by [1]

$$b(x,t) = \sum_{i=0}^{\infty} \hat{B}_i \cos(\nu_i x - \omega_i t - \Psi_i)\,, \tag{6}$$

where ν_i is the wave number, also called "number of pole pairs", and ω_i is the corresponding frequency of one particular wave. Applying (5) gives the force density in the air gap

$$\begin{aligned} p(x,t) \quad &= \frac{1}{2\mu_0}\left[\sum_{j=1}^{\infty} \hat{B}_j \cdot \cos(\nu_j x - \omega_j t - \Psi_j)\right]^2 \\ &= \frac{1}{2\mu_0}\sum_{k=1}^{\infty}\sum_{l=1}^{\infty} \hat{B}_k \hat{B}_l \cdot \cos(\nu_k x - \omega_k t - \Psi_k) \\ &\quad \cdot \cos(\nu_l x - \omega_l t - \Psi_l) \\ &= \frac{1}{2\mu_0}\sum_{k=1}^{\infty}\sum_{l=1}^{\infty} \frac{\hat{B}_k \hat{B}_l}{2} \\ &\quad \cdot \cos((\nu_l \pm \nu_k)x - (\omega_l \pm \omega_k)t - \Psi_l \pm \Psi_k) \\ &= \sum_{k=1}^{\infty}\sum_{l=1}^{\infty} \hat{P_{kl}} \cdot \cos(r_{kl}x - \omega_{kl}t - \Psi_{kl})\,. \end{aligned} \tag{7}$$

with

$$\hat{P_{kl}} = \frac{\hat{B}_k \hat{B}_l}{2\mu_0}, \quad r_{kl} = \nu_l \pm \nu_k, \quad \omega_{kl} = \omega_l \pm \omega_k, \tag{8}$$

Force waves combine magnetic flux density waves two by two. As the wave numbers of the force waves are strongly related with the vibrational eigenmodes of the stator, they are also called mode numbers.

One common method to analyze magnetic force density waves is Jordan's combination table [1], by which the air gap field $b(x,t)$ is calculated from the permeance function of the machine and the magnetomotive forces(MMF). As shown in Table I, the causes of typical air gap field harmonics can be derived. The wave numbers of harmonics excited by stator or rotor slotting, winding distribution or saturation are well known and described by the number of stator and rotor slot N_1 and N_2, the number of pole pairs p, the frequency of the fundamental component f_p. Simplifying assumptions and effects like saturation diminish the accuracy of quantitative statements concerning the amplitude of higher harmonics. In addition, it happens in practice that force density harmonics are obtained by FE analysis, that were not identified by the analytical model.

TABLE I: WAVE NUMBERS AND FREQUENCIES OF TYPICAL AIR GAP FIELD HARMONICS.

Cause	Wave number ν	Frequency order ω/ω_0
Stator slotting	$gN_1 + p, g \in \mathbb{N}$	1
Rotor slotting (IM)	$gN_2 + p, g \in \mathbb{N}$	$1 + \frac{gN_2}{p} \cdot (1-s)$
Stator wind. distr.	$p(6g+1), g \in \mathbb{Z}$	1
Current harmonic μ	$p(6g+\mu), g \in \mathbb{Z}$	μ
Saturation	3p	3

III. ANALYSIS OF MAGNETIC FORCE DENSITY WAVES USING NUMERICAL SIMULATION DATA AND A CONVOLUTION APPROACH

In comparison to the analytical approach, a two-dimensional electromagnetic FEM simulation provides an accurate representation of the magnetic flux density distribution. The air gap field can be sampled in time and space and the Fourier series coefficients can subsequently be approximated by means of the DFT. Since many air gap field waves combinations have the same wave numbers, a magnetic force density harmonic is usually the geometrical sum of a number of pairs of air gap field harmonics. The common approach of applying Fourier analysis to the force densities does not provide information about this composition. Before discussing the presented approach, the two-dimensional DFT and the usage of space vectors is briefly reviewed.

A. Two-dimensional Fourier analysis

Say $T > 0$, $\omega = \frac{2\pi}{T}$ and $f : [0, 2\pi] \times [0, T] \to \mathbb{C}$ is a piecewise differentiable function. Then f can be represented by a Fourier series:

$$f(x,t) = \sum_{n=-\infty}^{\infty}\sum_{m=-\infty}^{\infty} c_{nm} e^{j(nx + m\omega t)}\,. \tag{9}$$

The complex coefficients of the Fourier series are determined by

$$c_{nm} = \frac{1}{2\pi T}\int_0^{2\pi}\int_0^T f(x,t) e^{-j(nx+m\omega t)} dt dx \tag{10}$$

The function f now be sampled at discrete locations in space

$$x_k = k\Delta x\,, \quad k \in \mathbb{Z}\,, \quad \Delta x > 0\,. \tag{11}$$

and discrete instants in time

$$t_l = l\Delta t\,, \quad l \in \mathbb{Z}\,, \quad \Delta t > 0 \tag{12}$$

If in addition, f is periodic in space and is sampled N times ($2\pi = N\Delta x$) and if it is also periodic in time with M sample points ($T = M\Delta t$), then the function can be completely described by a matrix $Y \in \mathbb{C}^{N\times M}$. For the sake of simplicity $N, M \in \mathbb{N}$ be odd.

The two-dimensional discrete Fourier transform (2D-DFT), as approximation for the Fourier series of the function is defined as unique invertible linear mapping 2D-DFT : $Y \in \mathbb{C}^{N\times M} \to \bar{Y} \in \mathbb{C}^{N\times M}$ by means of the spectral coefficients:

$$\bar{c}_{nm} = \frac{1}{NM}\sum_{k=0}^{N}\sum_{l=0}^{M} y_{kl} e^{-j(nx_k + mt_l)}\,, \tag{13}$$

where y_{kl} are entries of the matrix $Y \in \mathbb{C}^{N\times M}$ and $\bar{y}_{nm}$ are entries of the matrix $\bar{Y} \in \mathbb{C}^{N\times M}$. The inverse mapping is called the two-dimensional inverse Fourier transform (2D-IDFT) and is defined by

$$y_{kl} = \sum_{n=0}^{N-1}\sum_{m=0}^{M-1} \bar{y}_{nm} e^{j(nx_k+mt_l)} . \tag{14}$$

There are algorithms, such as the Fast Fourier Transform [8] that efficiently compute (13) and (14).

The matrix Y approximates the function f, and $\bar{Y}$ its spectrum. If f is real, i.e. $y_{nm} \in \mathbb{R}\,\forall n, m$, then it can be written in the following form:

$$f(x,t) \approx \sum_{n=0}^{N-1}\sum_{m=0}^{M-1} A_{nm}\cos(nx + m\omega t + \varphi_{nm}) \tag{15}$$

This can be split into three parts:

$$\begin{aligned} f(x,t) \approx &\frac{a_{00}}{2} + \sum_{n=1}^{(N-1)/2} A_{n,0}\cos(nx + \varphi_{n,0}) \\ &+ \sum_{n=0}^{N-1}\sum_{m=1}^{(M-1)/2} A_{nm}\cos(nx + m\omega t + \varphi_{nm}) \end{aligned} \tag{16}$$

Therein, a_{00} corresponds to the DC component and zero order mode of the function f, A_{n0} are all DC components of the space harmonics. The remaining entries, e.g. $A_{n,m}\,\forall m = 1\ldots(M-1)/2, n = 0\ldots N-1$, determine the time and space harmonic waves of f. Therefore, only the latter term of (16) is relevant for vibration analysis, as it can represent forward and backward traveling waves. Note that this double sum ranges from 1 to only $(M-1)/2$ which means, that the transformed matrix $\bar{Y}$ only contains half as much entries as Y. However, these entries are complex in contrast to the entries of Y, which have been assumed to be real. Practically, that means only positive frequencies, but positive and negative wave numbers occur. Of course, the definition could also be chosen to have positive and negative frequencies and only positive wave number. The first convention is used in this paper.

The coefficients in (15) and (16) are determined by

$$a_{nm} = c_{nm} + c_{(N-n)(M-m)} \tag{17}$$

$$b_{nm} = j(c_{n,m} - c_{(N-n)(M-m)}) \tag{18}$$

$$A_{nm} = \sqrt{(a_{nm})^2 + (b_{nm})^2} \text{ and} \tag{19}$$

$$\varphi_{n,m} = \arctan\left(\frac{b_{nm}}{a_{nm}}\right) . \tag{20}$$

B. Concept of space vectors

Space vectors are frequently used as a tool to describe and calculate the flux model of vector controlled electrical machines under various operation modes. However, space vectors offer also a more general description for arbitrary one-dimensional harmonic waves in electrical machines. A graphic definition of space vectors defined as complex numbers was first proposed for electrical machines by Kovcs and Štěpina. It allows a handling of harmonic waves in a convenient way [9]. A single harmonic

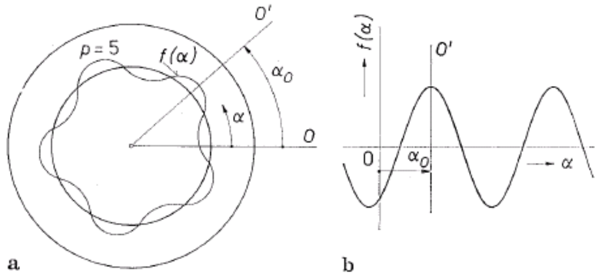

Figure 1. General illustrations of one-dimensional harmonic waves,(a) wave with p=5, (b) value along angle, from [9].

wave can be expressed by

$$\begin{aligned} f(\alpha) &= F_p \cdot \cos[p(\alpha - \alpha_0) + \omega(t - t_0)] \\ &= F_p \cdot Re\{e^{j(p\alpha_0+\omega t_0)} e^{-j(p\alpha+\omega t)}\}. \end{aligned} \tag{21}$$

The space vector is defined as the complex number

$$\underline{F} = F_p \cdot e^{j(p\alpha_0+\omega t_0)}. \tag{22}$$

In this way, the air gap field and magnetic force waves can be described by rotating vectors in the complex plane. The magnitude of the vector corresponds to the wave amplitude, whereas the angle corresponds to the phase shift as depicted in Figure 1.

C. Convolution approach

In the sampling procedure in space and time, a full period and a full revolution of the FEM solution data is stored into matrix B. In order to consider the magnetic force density waves, the magnetic force density matrix P is created by applying (5) to each matrix entry b_{kl}. Subsequently, a two-dimensional DFT of P provides the approximated Fourier series coefficient $\bar{p}_{nm}$. Path $(B, P, \bar{P})$ in Figure 2 illustrates this approach. The matrix $\bar{P}$ contains space vectors of harmonic magnetic force waves.

Path $(B, \bar{B}, \bar{P})$ in Figure 2 indicates an alternative way of calculating magnetic force density waves $\bar{P}$. First, the 2D DFT is applied directly to the air gap field matrix B. Then, $\bar{P}$ is obtained by matrix convolution. The two-dimensional periodic matrix convolution

$$Z = X * Y \tag{23}$$

of two given matrices $X, Y \in \mathbb{C}^{K\times L}$ is defined by

$$z_{s,t} = \sum_{k=1}^{K}\sum_{l=1}^{L} y_{k,l} \cdot y_{s-k,t-l} , \tag{24}$$

It can be shown that a multiplication in time domain, e.g. B^2 corresponds to a convolution in frequency domain, e.g. $\bar{B} * \bar{B}$ [8].

$$\begin{tikzcd} B \arrow[r, "\text{2D-DFT}"] \arrow[d, "\cdot"] & \bar{B} \arrow[d, "*"] \\ P \arrow[r, "\text{2D-DFT}"] & \bar{P} \end{tikzcd}$$

Figure 2: Commutative diagram.

TABLE II: CONTRIBUTING AIR GAP FIELDS.

$r = -2; \quad \omega/\omega_0 = 2$
$p_{tot} = 24556\,\text{N/m}^2 < 115^o$

Space vector	ω/ω_0	ν	ω/ω_0	ν
A	2	-2	4	-4
B	4	-4	6	-6
C	1	-1	5	-3
D	3	-3	5	-5
E	1	-1	1	-1

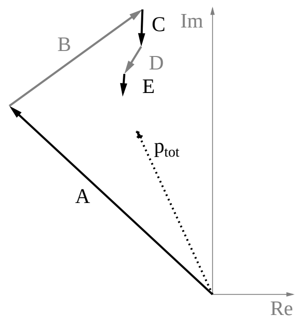

Figure 3. Space vector diagram for $r = -2$ and $\omega/\omega_0 = 2$.

Applied to the air gap field DFT matrix, a periodic matrix convolution combines all matrix entries with each other:

$$\bar{P} = \frac{1}{2\mu_0} \cdot \bar{B} * \bar{B}. \tag{25}$$

This approach seems to be complex and costly. A complete convolution (24) would indeed be very time consuming. However, a complete convolution is not necessary since only a very small number of combination pairs do contribute significantly to the magnetic force density wave that really cause audible noise. Therefore, only the matrix entries of $\bar{b}_{nm}$, whose amplitude exceed a chosen threshold need to be considered in the calculation.

The advantage of this approach in contrast to path $(B, P, \bar{P})$, arises from the fact that each air gap field convolution pair is known and can be stored. Thus, for each resulting force density wave $\bar{p}_{nm}$ a set of pairs

$$\bar{p}_{nm} : \{(\bar{b}_{n_1m_1}, \bar{b}_{n_2m_2}); (\bar{b}_{n_3m_3}, \bar{b}_{n_4m_4}); \ldots\} \tag{26}$$

is stored.

As an example result of such calculation, Table II shows the largest five contributions to the second order, mode two, excitation force density wave. The wave numbers and frequency orders must be added or subtracted to obtain $r = -2$ and $\omega/\omega_0 = 2$ according to (8).

D. Space vector diagram

Following the convolution approach (II), each magnetic force wave can be decomposed into the geometric addition of partial space vectors as shown in Figure 3, which represents the same data as Table II. The depicted magnetic force density wave has mode number $r = -2$ and and a frequency order of $\omega/\omega_0 = 2$. Each of the partial vectors A, B, C etc. is associated with an air gap field combination pair. The partial vectors are sorted according to their

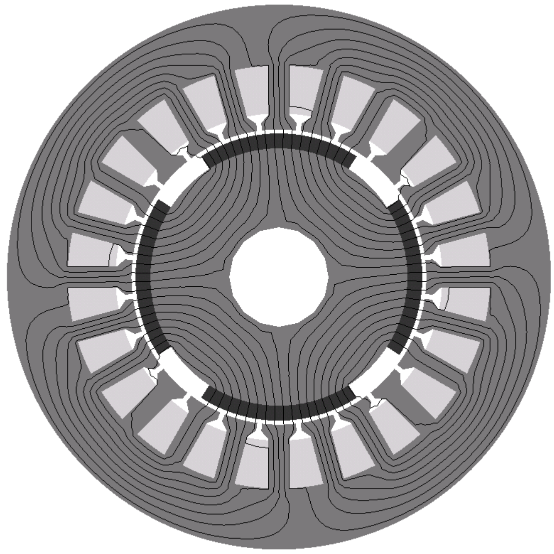

Figure 4. Stator and rotor of four pole example PMSM with field lines.

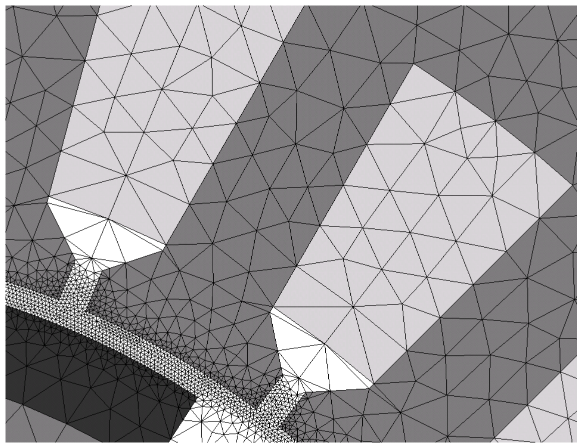

Figure 5: FE mesh.

magnitude. The broken line is the total magnetic force density vector calculated using path $(B, P, \bar{P})$. Obviously, the chain of partial vectors adds up to the total vector. A truncation error that depends on the chosen convolution threshold and on the number of stored partial vectors leads to a gap between the total vector and the vector chain.

IV. NUMERICAL RESULTS

A. Example machine

To demonstrate the proposed method, a permanent magnet excited synchronous machine (PMSM) is investigated. It is designed using in-house software for the automated sizing of PMSM [10]. The machine data is shown in Table III. Its cross-section together with the field distribution in rated operation can be seen from Figure 4. Figure 5 shows the FE mesh, which is used.

The magnetic flux density is sampled in the air gap, this is done for each time step individually. The radial field for one time instance and its spatial spectrum can be seen from Figure 6 and 7, respectively. The spectrum of the resulting force density waves are shown in Figure 8. The convolution of the fundamental field with it self typically yields high amplitudes, in this case it is 162775 N/m^2. The scale of Figure 8, however, was chosen to clearly depict

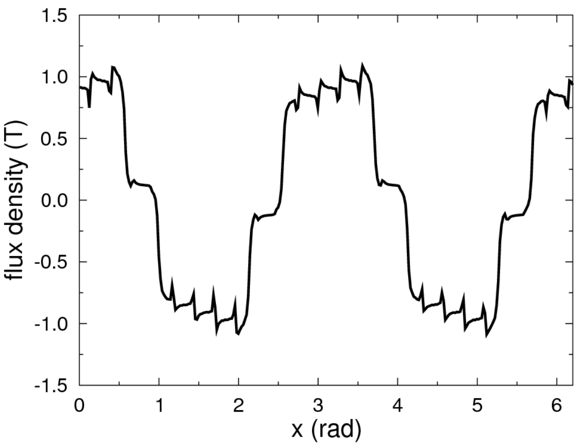

Figure 6: Radial air gap flux density.

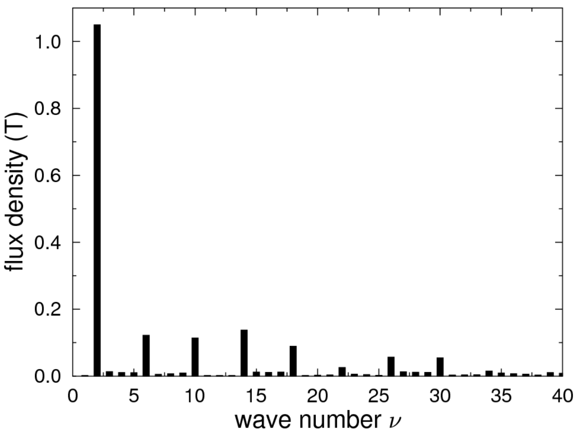

Figure 7: Radial air gap flux density spectrum.

the most relevant higher force density harmonics of modes r=0,2 and 4 and only the maximum amplitude of the positive and negative modes is chown.

The convolution approach is applied to the air gap field sampled in time and space. As a first example, the second temporal order, mode 4 force density harmonic, which is supposed to be excited by the fundamental field convoluted by itself, is analyzed. All flux density waves that are larger than 0.01% of the fundamental field are considered as convolution partners. The space vector diagram of Figure 9 shows the three most relevant partial space vectors. Their wave numbers and orders are given in Table IV. The fundamental field squared (A) adds by far the largest contribution, however, at least one more flux density wave (B) shows some minor influence.

TABLE III: MACHINE DATA OF THE EXAMPLE PMSM.

Machine data	Value
Number of pole pairs p	2
Rated power P_n	2 kW
Rated speed n_n	4500 rpm
Rated voltage V_n	230 V
Rated current I_n	11.2 A
Outer stator diameter D_o	110 mm
Inner stator diameter D_i	60 mm
Mechanical air gap δ	0.8 mm
Active length l_{Fe}	120 mm
Number of stator slots N_1	24

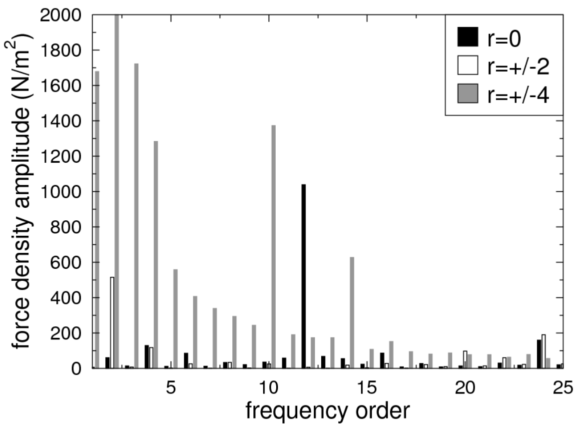

Figure 8: Force density amplitude of different modes.

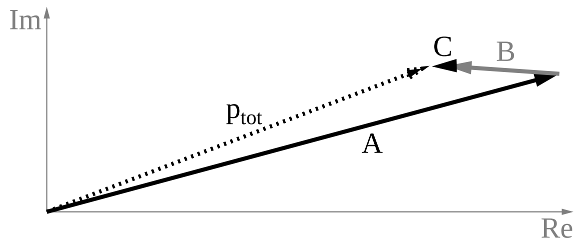

Figure 9. Space vector diagram for $r = -4$ and $\omega/\omega_0 = 2$.

As a second example, the 12th temporal order, mode 0 force density is considered. As illustrated in Figure 8 this harmonic has a significantly lower amplitude of 1042 N/m^2, but is still among the most significant higher frequency orders. The space vector diagram of Figure 10 shows a different geometric addition. The force wave is not determined by only one partial vector, but it contains significant at least two equally significant partial vectors A and B. The wave numbers and frequency orders are given in Table V. A small gap between the total force density vector and the sum of the vectors A to F show the asymptotic nature of the proposed method. The wave numbers and frequency orders of the considered force density waves are summarized in Table II. Further application examples of the proposed method can be found in [11].

B. Comparison with full stress tensor calculation

To justify the approach and to investigate its limits, the force density in mode/frequency domain obtained from stress tensor using (1), which would be typically used for a subsequent structural dynamic simulation, is compared to the simplified formula (5). Figure 11 shows the relative

TABLE IV: CONTRIBUTING AIR GAP FIELDS.

$r = -4; \quad \omega/\omega_0 = 2$
$p_{tot} = 170258\,\text{N/m}^2 < 21^o$

Space vector	ω/ω_0	ν	ω/ω_0	ν
A	1	-2	1	-2
B	1	-2	3	-6
C	5	-10	7	-14

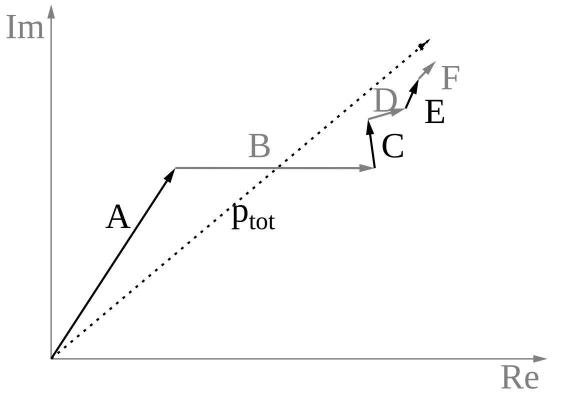

Figure 10. Space vector diagram for $r = 0$ and $\omega/\omega_0 = 12$.

TABLE V: CONTRIBUTING AIR GAP FIELDS.

$r = 0$; $\omega/\omega_0 = 12$
$p_{tot} = 1042\,\text{N/m}^2 < 40^o$

Space vector	ω/ω_0	ν	ω/ω_0	ν
A	1	-26	13	-26
B	1	-2	11	2
C	1	-2	13	-2
D	5	14	7	-14
E	3	18	9	-18
F	3	-30	15	-30

deviation between those two. For the fundamental field square, its magnitiude is used as reference value, for all other waves, 2000 N/m^2 is used as reference value, which corresponds to the maximum amplitude shown in Figure 8. The deviation of the angle between the calculation using (1) and (5) is shown in Figure 12 for all waves with an amplitude larger than 600 N/m^2, which is less than 0.5% of the amplitude of the fundamental field squared. It can be seen that the relative error is below 40% and the angle error is less than 30^o for all shown harmonics. The deviation is still significant as to still use the full stress tensor calculation for the excitation of precise structural dynamic simulations, however, the obtained accuracy can be considered sufficient for studying the contributions of the individual flux density waves to a particular force wave.

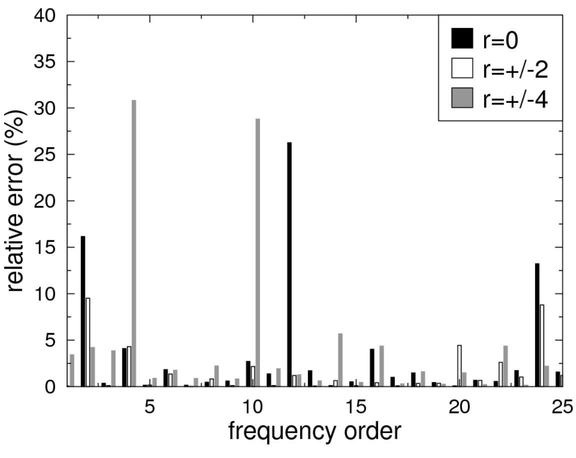

Figure 11: Deviation between MST and $B^2/2\mu_0$.

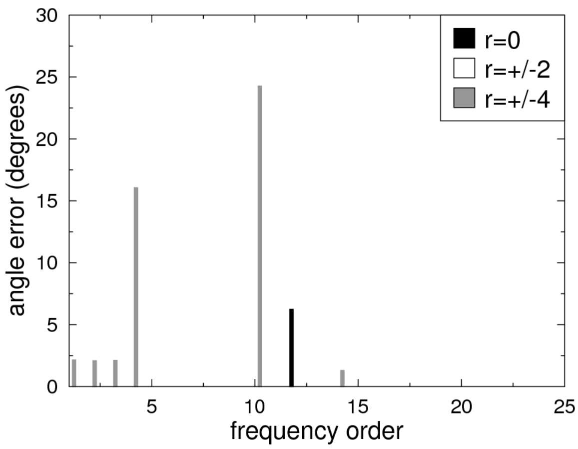

Figure 12: Deviation between MST and $B^2/2\mu_0$.

V. SUMMARY AND CONCLUSIONS

The method presented in this paper allows the determination of the contributions of partial force density waves to a specific force density waves. The approach is based on the 2D Fourier transform representation of the magnetic flux density in the air gap and its convolution with itself. It is shown that the convolution can be limited to the computation of the most relevant matrix entries. As an example, the air gap field and the force density waves of a PMSM are analyzed to demonstrate the effectiveness of the proposed approach. For this example, the error between the full stress tensor calculation and its simplified version is analyzed. The error is not negligible, but is still small enough to apply the proposed approach in noise and vibration diagnosis of electrical machine.

REFERENCES

[1] H. Jordan, *Geräuscharme Elektromotoren*, H. Franz, Ed. W. Girardet, November 1950.

[2] J. Gieras, C. Wang, and J. C. Lai, *Noise of Polyphase Electric Motors*. CRC Press Taylor&Francis Group, 2006.

[3] M. Furlan, A. Cernigoj, and M. Boltezar, “A coupled electromagnetic-mechanical-acoustic model of a dc electric motor,” *COMPEL: The International Journal for Computation and Mathematics in Electrical and Electronic Engineering*, vol. 22, no. 4, pp. 1155–1165, 2003.

[4] C. Schlensok, B. Schmülling, M. van der Giet, and K. Hameyer, “Electromagnetically excited audible noise evaluation and optimization of electrical machines by numerical simulation,” *COMPEL: The International Journal for Computation and Mathematics in Electrical and Electronic Engineering*, vol. 26, pp. 727 – 742, 2007.

[5] T. Kobayashi, F. Tajima, M. Ito, and S. Shibukawa, “Effects of slot combination on acoustic noise from induction motors,” *Magnetics, IEEE Transactions on*, vol. 33, no. 2, pp. 2101–2104, 1997.

[6] F. Henrotte and K. Hameyer, “A theory for electromagnetic force formulas in continuous media,” *Magnetics, IEEE Transactions on*, vol. 43, no. 4, pp. 1445–1448, April 2007.

[7] J. Melcher, *Continuum Electromechanics*. MIT Press Cambridge Massachusetts, 1981.

[8] A. Oppenheim, R. Schafer, and J. Buck, *Discrete-Time Signal Processing*, 2nd ed. Prentice Hall, 1999.

[9] J. Štěpina, “Komplexe Größen in der Elektrotechnik,” *Electrical Engineering (Archiv für Elektrotechnik)*, vol. 72, no. 6, pp. 407–414, November 1989.

[10] M. Hafner, M. Schöning, and K. Hameyer, “Automated sizing of permanent magnet synchronous machines with respect to electromagnetic and thermal aspects,” in *Proceedings of the 2008 International Conference on Electrical Machines*, 2008.

[11] M. van der Giet, R. Rothe, M. Herranz Gracia, and K. Hameyer, “Analysis of noise exciting magnetic force waves by means of numerical simulation and a space vector definition,” in *Proceedings of the 2008 International Conference on Electrical Machines*, 2008.